Received: 27 October 2016 | Accepted: 23 March 2017
DOI: 10.1111/ijag.12272

ORIGINAL ARTICLE

INTERNATIONAL JOURNAL OF Applied Glass SCIENCE

Direct observation of crack propagation in a liquid crystal display glass substrate during wheel scribing

Naoko Tomei[1,2] | **Kumiko Murakami**[1] | **Toshio Fukunishi**[1] | **Satoshi Yoshida**[2] | **Jun Matsuoka**[2]

[1]Research & Development Department, Mitsubishi Diamond Industrial Co., Ltd., Settsu, Japan

[2]Department of Materials Science, The University of Shiga Prefecture, Hikone, Japan

Correspondence
Naoko Tomei
Email: ntomei@mitsuboshi-dia.co.jp

Abstract

In-situ observation of crack propagation in an LCD glass substrate was performed during wheel scribing. It was found that a median crack initiated just beneath the wheel and stopped once, and that the crack re-propagated after passing through the wheel. In this study, the first pop-in median crack is defined as the first crack, and the re-grown median crack is defined as the second crack. From in-situ photoelastic measurements during a static indentation of the wheel, the maximum tensile stress was observed just beneath the wheel. The tensile stress beneath the wheel was also confirmed from FE analysis. It is considered that this tensile stress is the origin of the first crack nucleation. On the other hand, from post-observation of the cross-section of a scribing groove after scribing, it was found that the median crack was closed in the plastic zone. It is considered that this closure results from compressive stress in the plastic zone beneath the scribing groove, and that this compressive stress causes the first crack to be arrested.

KEYWORDS

FE analysis, in-situ photoelastic measurements, median crack propagation, wheel scribing

1 | INTRODUCTION

Recently, thickness of LCD (Liquid Crystal Display) glass substrate becomes thinner and thinner year by year due to high demand for thinner and lighter laptop or mobile device. Therefore, it is of primary importance for cutting such a thin sheet glass with high efficiency. It is also known that edge quality of glass substrate after machining affects strength of the glass. In order to supply glass substrates with reliable strength, it is important to get a deeper insight into mechanism of machining or cutting of the glass sheet.

In general, "scribing+breaking" technique is employed for cutting LCD glass panels, because it is a high-speed dry process without kerf loss and with less thermal damage. In the scribing process, a cutting tool called a scribing wheel is used. During the scribing process, the scribing wheel creates a groove on the glass substrate, and a median crack initiates at the bottom of the groove. In the breaking process, bending stress causes the median crack to propagate further, and the glass substrate is separated into two. If geometries of the scribing wheel and scribing conditions are not suitable for the scribing and breaking processes for a given glass sheet, undesirable cracks, such as a lateral crack or chipping may be generated. Such fault cutting results in unfavorable low strength of the glass.[1,2] However, there are less information available on effects of scribing conditions and/or wheel geometries on the edge quality of glass substrate.

On the contrary, there are many studies on crack initiation and propagation in glass during quasi-static indentation using a diamond indenter. It is known that some characteristic cracks, such as a ring crack, a radial/median crack, and a lateral crack are generated during an indentation cycle.[3,4] The type of crack observed depends both on glass composition and on indenter geometries. In scribing process, on the other hand, the most important and "favorable" crack is the median crack, because the crack propagates in the direction of thickness as described above. It has been reported that the median crack during quasi-static indentation nucleates on loading.[5-7] Indentation induces tensile stress under the plastic zone, which is the plastically deformed region.[8,9] Under a load of indentation, the median crack stays inside the glass due to the compressive stress at surface. During unloading, on the other hand, the tensile stress at the bottom of the plastic zone changes into compressive, and the stress at surface becomes tensile. This is the reason that the median crack grows into the radial crack at surface.[4,10] In addition, the CME (Chiang, Marshall, and Evans) model[11] also explains various cracking sequences during the indentation cycle. For example, the CME model confirms that the stress pertinent to radial cracking is surface localized, and that the stress increases during unloading half cycle. The CME model also shows that the maximum stress for median cracking is less than that for radial cracking. It also supports an importance of radial cracking during quasi-static indentation cycle. On the other hand, shear band formation within the plastic zone beneath an indenter has been reported.[12] It was suggested that hardening effect was presented from observation of void or crack formation at the intersection points or along the flow lines, and that the shear band is the origin of the median crack initiation.

As compared with the indentation-induced cracking, it is still unclear where and when the median crack during scribing initiates and how it propagates. There is one report where surface stress and internal stress of PMMA (poly-methyl-methacrylate) and photoelastic sensitive material, CR-39 (Ethylene glycol bis(3-butenoate)) are successfully visualized during a static contact with an aluminum wheel.[13] Another report by the same authors[14] shows polarized images of soda-lime glass under a static indentation of a steel wheel. Unfortunately, however, the obtained stress field is not quantitative due to limited resolution of the polarized images. There are other reports which show the relationship between the median crack depth and the geometries of the wheel.[14-19] The median crack depth decreases with an increase in the tip angle or in the wheel diameter. In addition, the contact mechanics of sharp "glass-cutting" rollers has been analyzed. Cook showed that the residual constrained deformation of the wheel groove by rolling was the driving force for median cracking.[19] Cook estimated the lengths of median cracks generated by rolling contacts, and confirmed that they were in good agreement with observations. Although the relation reported is of primary importance for high efficient cutting of a glass sheet, these papers[15,16] focused only on the post observation of the crack accompanied with the scribing groove. Recently, micro-photoelastic observations around the indentation imprint were reported for strengthened glass[20] and for silica and soda-lime glasses[21] after and/or during indentations. This micro-photoelastic technique has been applied to observation of a glass substrate during wheel scribing.[22] Although the authors[22] suggest that the in-situ photoelastic measurement would be a useful tool for in-process management of the edge quality of a glass substrate, the detail mechanism of crack propagation during wheel scribing has not been clarified yet.

In this study, in-situ observation during wheel scribing and post observation of the scribing groove were performed in order to clarify the mechanism of crack propagation during wheel scribing. In addition, in-situ photoelastic measurement and FE analysis were conducted to estimate stress distribution during wheel scribing.

2 | EXPERIMENTAL PROCEDURE

Figure 1 shows a schematic illustration of a lab-made scribing equipment. A glass plate was placed on the sample stage, which was stationary and equipped with a vacuum chuck in order to fix the sample. As shown in Figure 1, a scribing wheel can move in the direction of Y-axis from left to right during scribing. The scribing wheel (Figure 2A) with an axle was inserted into a wheel holder (Figure 2B), and the wheel holder was attached to a movable stage shown in Figure 1.

The scribing wheel and the axle were not locked to the wheel holder, thus both could rotate freely. The scribing wheel used in this study had a diameter, D of 2.0 mm, an inside diameter, H of 0.8 mm, a thickness, T of 0.65 mm, and a tip angle of the wheel, V of 130°, respectively. Also, the scribing wheel was made of sintered Tungsten Carbide (WC) alloyed with 5.0 wt% of Co.

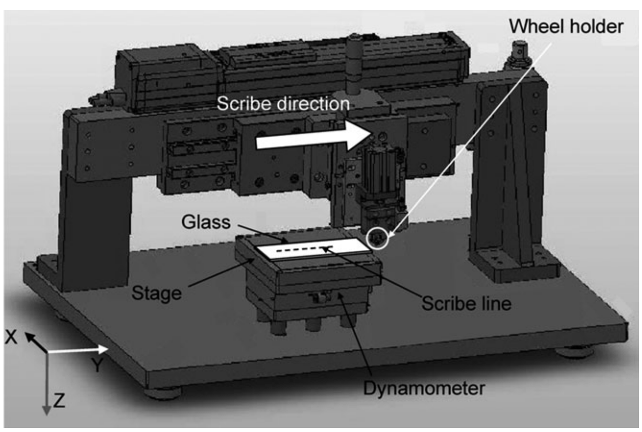

FIGURE 1 Schematic illustration of a scribing equipment

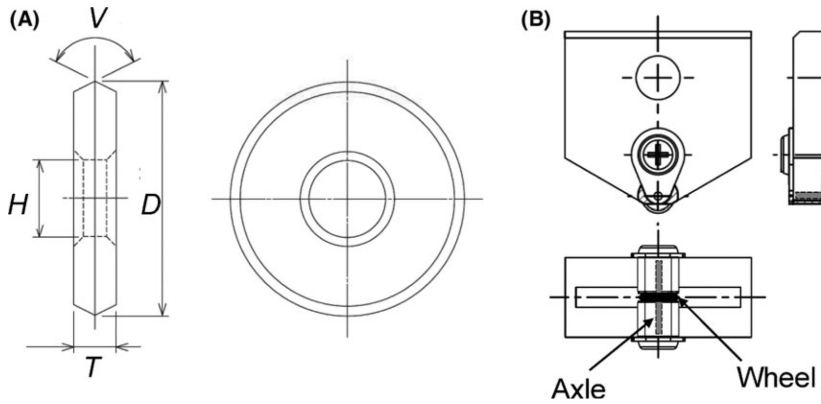

FIGURE 2 Schematic illustrations of scribing components, (A) Wheel and (B) Wheel holder

The normal force during scribing was controlled by air pressure. In order to keep a constant normal force during scribing, the wheel holder was allowed to move up and down due to surface waviness of the glass sample. The scribing speed was constant at 10 mm/s. The normal force during scribing was monitored using a three-dimensional dynamometer (9119AA2; Kistler, Winterthur, Switzerland) which was attached under the sample stage. The sampling rate of the three force components was 2000 Hz. The scribing force, Fz, or the normal force during scribing, was determined as the mean value of the forces in the direction of *Z*-axis during the scribing of 50 mm. The scribing force was kept constant during scribing, and increased stepwise from 3.13 N to 24.6 N. The standard deviation of the scribing force, Fz varied from 3.46% for Fz=3.13 N to 0.52% for Fz=24.6 N. The glass sample used in this study was non-alkaline (alkaline earth boro-aluminosilicate) glass (Eagle XG; Corning Inc., NY) with a thickness of 0.7 mm for an LCD glass panel. The dimensions of the glass plate used were *L* (length) 50 mm×*W* (width) 100 mm×*T* (thickness) 0.7 mm for measurements of median crack depth.

Figure 3 shows a schematic illustration of in-situ observation system with a high speed camera (FASTCAM MH-4; Photron, Tokyo, Japan). The high speed camera was clamped on a tripod stand separated from the scribing equipment, therefore the in-situ observation images of crack propagation during scribing could be recorded at a fixed-point. The observation was performed from the negative direction of *X*-axis with the transmitted light from the light source on the opposite side of the camera. The optical pass length through the glass sample was 20 mm. The shooting speed of high speed camera was 500 frames-per-second (fps).

In order to estimate the stress field of the glass sample under a static wheel indentation, retardation, and fast axis orientation were also measured with a polarization camera (FASTCAM MC2.1P; Photron). Figure 4 shows a schematic illustration of in-situ observation system for the photoelastic behavior. The photoelastic measurement was performed from the direction of the wheel edge (from the negative direction of *Y*-axis). The dimensions of the glass plate used were L (length) 20 mm×W (width) 20 mm×T (thickness) 0.7 mm for in-situ observation and photoelastic measurement. The retardation and the fast axis orientation at each pixel were determined from four kinds of polarization images obtained at different analyzer angles (0, 45, 90, 135 degrees). The incident light was the circularly polarized light with a wavelength of 520 nm. The shutter speed of a polarization camera was 500 μs, which includes the closure time of the shutter. Thus, the actually exposure time was 498 μs. The retardation and azimuth in the photoelastic observation system were determined per imaging pixel. Therefore, the spatial resolution corresponds to the pixel size which is 2.4×2.4 μm.

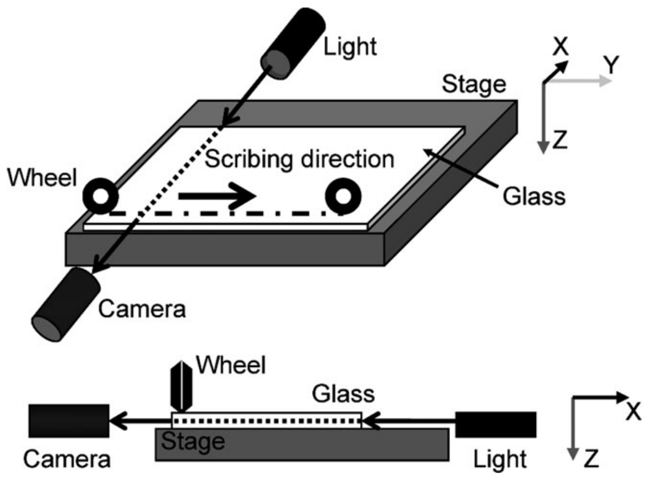

FIGURE 3 Schematic illustration of in-situ observation system with a high speed camera

After scribing, a scribing groove and cracks were observed using an optical microscope (VHX-1000; KEYENCE, Osaka, Japan), and a laser microscope (VK-9700; KEYENCE). Magnified images of the cross-sectional plane perpendicular to the scribing groove were obtained using an SEM (S-3400N; Hitachi High-Technologies, Tokyo, Japan). The cross-sectional plane was prepared using a

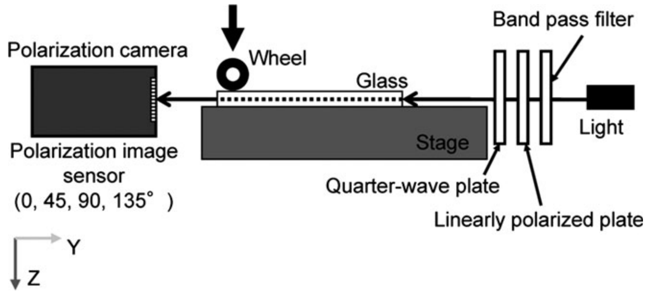

FIGURE 4 Schematic illustration of in-situ observation system for photoelastic measurements

Focused Ion Beam (FIB E-3500; Hitachi High-Technologies).

To discuss validity of the result of photoelastic experiments, the stress field under a scribing wheel was calculated with Finite Element Analysis (FEA). Table 1 shows the parameters used for the FEA (ANSYS, Canonsburg, PA). Figures 5A and B show the mesh patterns of the FEA. Figure 5A shows quarter size of the model, and 5B shows an enlarged view of the model. The FEA calculation was performed for an elasto-plastic material, and determined the three-dimentional stress field. The minimum of mesh-size around the contact point was 2 μm, the outer mesh-size was 20 μm. The sample size in the FEA model is 1 mm wide which is smaller than experimental size, 20 mm wide. However, the model size is large enough, because the stressed region (Figure 12) is limited within about 30 μm from the center of the indentation.

Yield stress and a work-hardening coefficient shown in Table 1 were determined from the load-depth curve for the Berkovich indentation.[23] At first, the load-depth curves were measured by experimental indentation. The two parameters were determined as fitting parameters of the curves, assuming that stress-strain relationship could be approximated by two straight-lines using "Isotropic Hardening rule[24]". The bottom and side faces of the mesh pattern were constrained in vertical directions to each face. The FEM simulations were quasi-static implicit. Loading and unloading speed were 0.64 N/s, the maximum load was 6.4 N, and holding time was 1 second. Rate-dependent plasticity, viscoelasticity and creep behavior were excluded in the present simulation. In addition, permanent densification of glass was not considered in this calculation.

TABLE 1 Parameters of FEA

Young's modulus (GPa)	Poisson's ratio	Mass density (kg/m^3)	Yield stress (GPa)	Work-hardening coefficient (GPa)
70	0.203	2520	3.5	1

3 | RESULTS

Figures 6A and B show the cross-section plane perpendicular to the scribing groove and the cutting plane after scribing at 24.6 N, respectively. It is found that the median crack propagated in the thickness direction without branching (Figure 6A). In Figure 6B, on the other hand, two kinds of arrest-lines of the median crack can be observed after scribing. These arrest-lines suggest that the median crack was arrested once, and re-propagated again. In this paper, the first pop-in median crack and the re-grown median crack are defined as the first crack and the second crack, respectively.

Figure 7 shows a relationship between crack depth and scribing force, Fz. The crack depths were determined from the arrest lines of cutting plane (Figure 6B). The error bars shown in Figure 7 represent±1 SD, which was determined from 10 scribing tests under an identical condition. However, the error bars of the first crack depth and Fz are omitted, because they are smaller than the symbols. The crack depths of the first crack and the second crack increase with an increase in scribing force. It is found that the first crack initiates at around 5 N. Meanwhile, the second crack starts at around 21 N. In other words, both the 1st and the second cracks show their different threshold forces for propagation. In addition, the scribing force dependence of the depth of the second crack is much larger than that of the first crack. The maximum depth of the second crack is more than 500 μm, which is about 70% of the sample thickness, 0.7 mm.

In order to evaluate crack initiation behavior during scribing, in-situ observation was performed using a high speed camera. Figure 8 shows some snapshots of the glass during scribing at 24.6 N. The white small arrows in each snapshot indicate the position of crack tip. The markings of the bottom edge are not related to the scribing groove on the top surface. In order to obtain the cross-section of cutting plane, the reverse side of the scribing surface was scribed and broken by hands. Therefore, the markings were formed by scribing the reverse side. The crack depths in the frames of 0 second (Figure 8A) and 0.08 second (Figure 8B) are almost unchanged. It is considered that this corresponds to the arrest mark of the first crack as shown in Figure 6B. It is found that the maximum depth of the first crack is always located at just beneath the scribing wheel. After the wheel passes through the photo frame as shown in Figure 8C, the median crack propagates again, and grows deeper and reaches the constant depth as shown in the frame of 1.0 second (Figure 8D). This final depth corresponds to the arrest mark of the second crack (Figure 6B). It is also found in Figure 8D that the depth of the first crack becomes unclear after the second crack propagation.

As shown in Figure 8, it is found that the first crack initiates just beneath the wheel, whereas that the second crack propagates after the wheel passes by. In other words, the

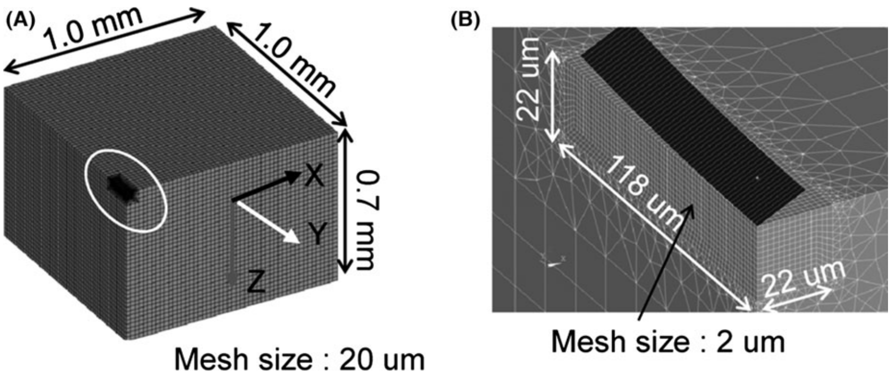

FIGURE 5 Mesh patterns of the FEA (A) Quarter size of the model, (B) Enlarged view of the model

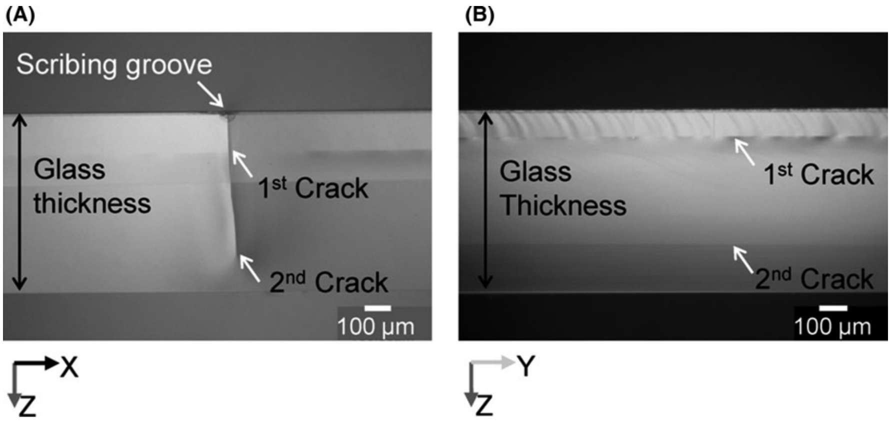

FIGURE 6 Microscope images of glass after wheel scribing at 24.6 N (A) Cross-section plane perpendicular to the scribe groove, (B) Cutting plane

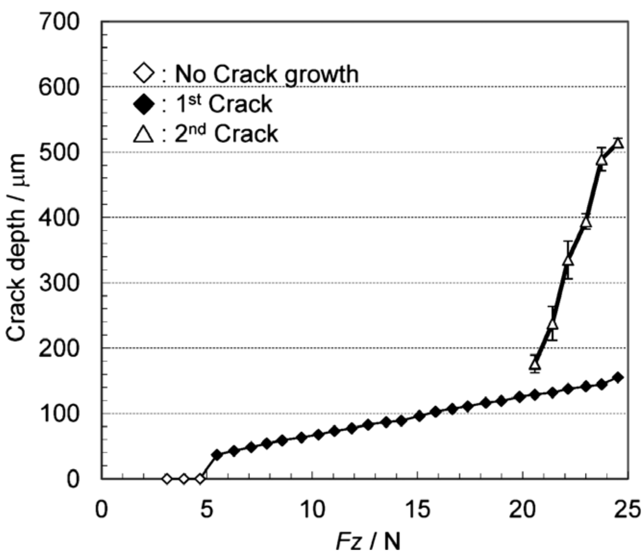

FIGURE 7 Relationship between crack depth and scribing load Fz

first crack grows under a load, and the second crack grows after unloading. In order to confirm it, in-situ photoelastic measurements were performed under a static indentation of the wheel.

The in-situ photoelastic image of the glass under a load of 6.4 N is shown in Figure 9. The color bar indicates the range of retardation values from 0 nm (blue) to 130 nm (red). The maximum of retardation in the glass is found in the point just beneath the wheel.

4 | DISCUSSION

Although the retardation shown in Figure 9 gives us information on the difference in principal stresses under a load, it cannot indicate whether the stress at a given point is compressive or tensile. However, the stress field can be calculated using the retardation and the fast axis orientation, assuming that the generated stress field is two-dimensional. The relationship between the retardation and the principal stress difference is defined as the following equation.[25]

$$R = Ct(\sigma_{11} - \sigma_{22}) \tag{1}$$

where R is the retardation, C is the photoelastic constant, t is the optical path length, σ_{11} and σ_{22} are the principal stresses.

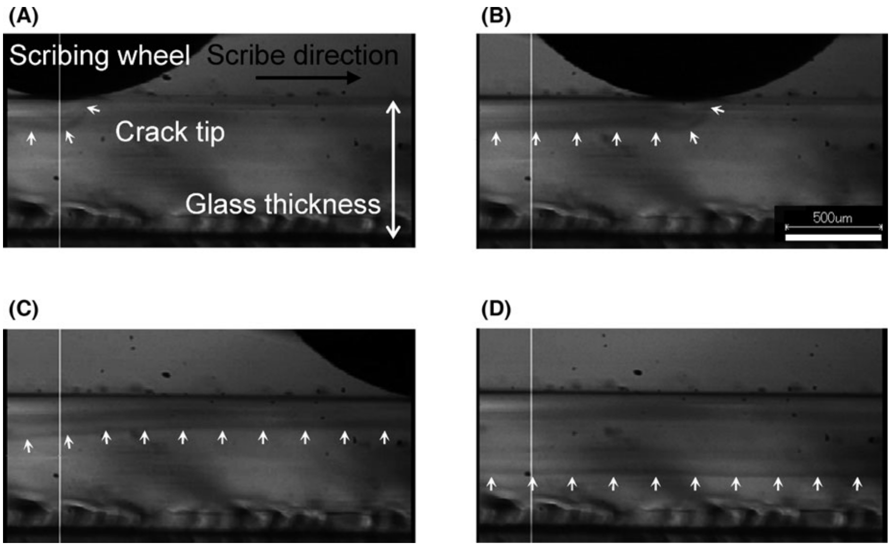

FIGURE 8 Snapshots during wheel scribing of a glass under a normal force of 24.6 N (A) 0 s, (B) 0.08 s, (C) 0.2 s, (D) 1.0 s

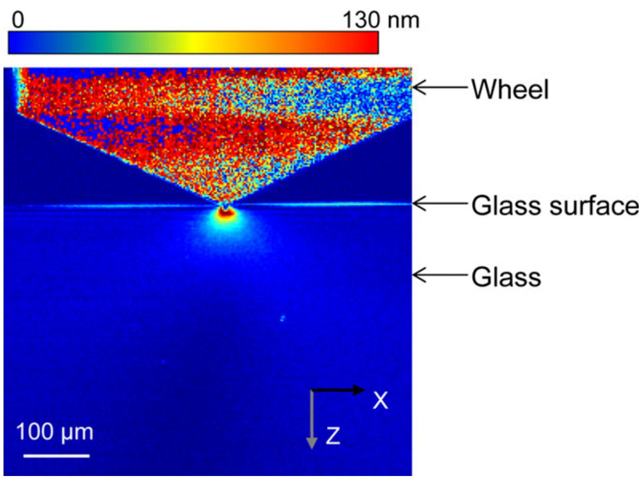

FIGURE 9 Retardation image during wheel indentation at 6.4 N

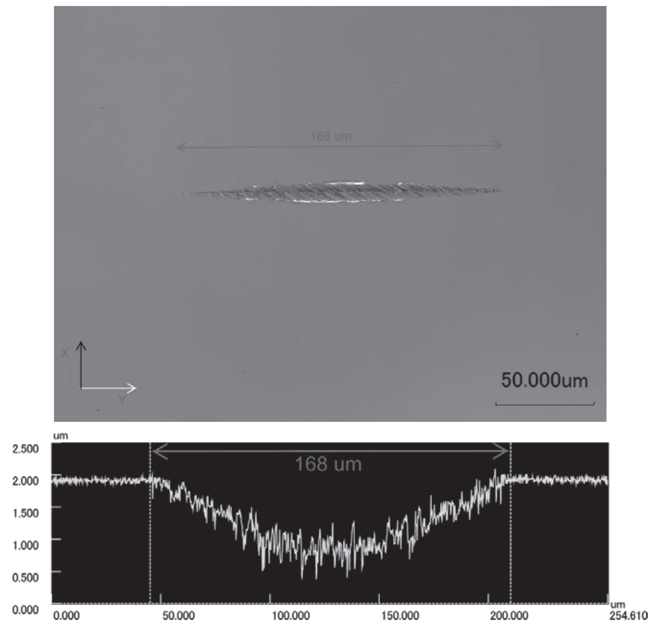

FIGURE 10 Top-view and cross-section profile of a residual imprint after wheel indentation at 6.4 N

In order to estimate the stress field of the glass sample beneath the wheel, the optical path length, t is required as shown in Equation 1. Therefore, the size of a residual imprint was measured after wheel indentation. The profile of the indentation imprint is shown in Figure 10. Due to the arc shape of the wheel, the stress field of the cross-sectional plane perpendicular to the direction of light pass (Y-axis) should be dependent of the Y-position. In order to simplify the stress field, however, it is assumed that the two-dimensional stress field in X-Z plane is identical at any Y-position of residual imprint whose length is 165 μm.

The retardation and the fast axis orientation (θ') were determined from photoelastic experiments. From the difference in principal stresses and the slow axis orientation (θ), which is obtained by subtraction 90° from θ', the shear stress (τ_{xy}) in the X-Y plane can be obtained by the following equation.[25]

$$\tau_{xy} = \frac{1}{2}(\sigma_{11} - \sigma_{22})\sin 2\theta \tag{2}$$

Using the obtained shear stress (τ_{xy}) and the equilibrium equations of two-dimensional stress field,[25] the other stress components are also obtained.

$$\sigma_x = (\sigma_x)_0 - \int_{x_0}^{x} \frac{\partial \tau_{xy}}{\partial y} dx \tag{3}$$

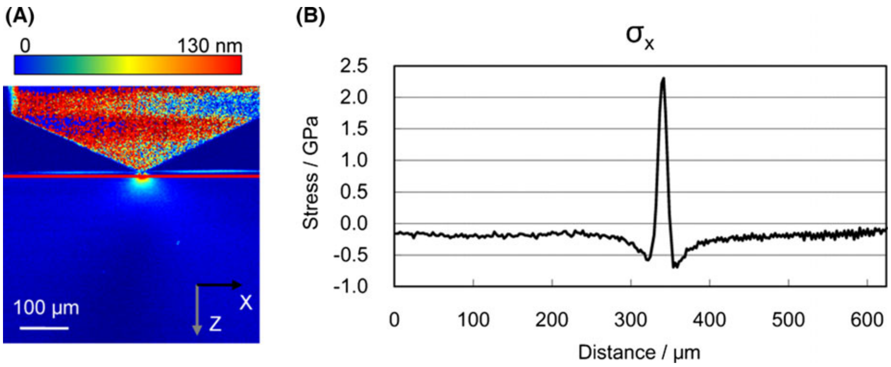

FIGURE 11 Retardation image (A) and σ_x stress distribution (B) on the red line in (A) calculated from Equations 1-3

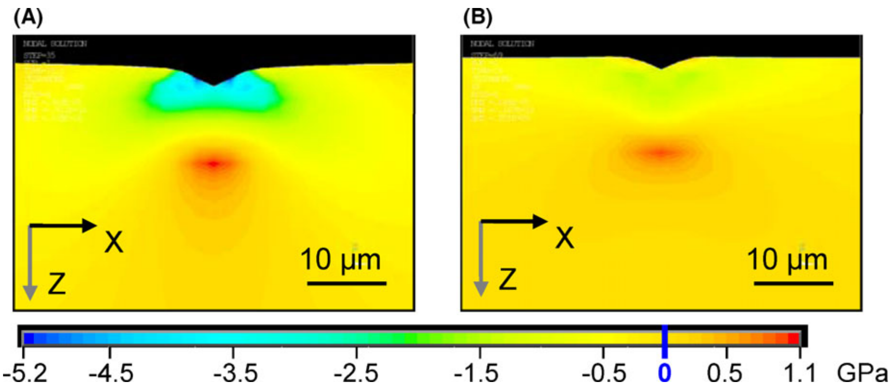

FIGURE 12 σ_x stress maps by FEA (A) during wheel indentation at 6.4 N and (B) after the indentation. The blue and red regions represent compressive and tensile stress, respectively

$$\sigma_y = (\sigma_y)_0 - \int_{y_0}^{y} \frac{\partial \tau_{xy}}{\partial x} dy \tag{4}$$

where x_0 and y_0 are the integral starting point, $(\sigma_x)_0$ and $(\sigma_y)_0$ are the normal stresses of the integral starting point, respectively.

Figure 11B shows the normal stress, σ_x, distribution calculated from the photoelastic image as a function of the distance, x, on the red line shown in Figure 11A. The width of red line in Figure 11A is about 7 μm, and the center of the line is located about 11 μm from the surface. As shown in Figure 11B, it is found that the maximum tensile stress which is about 2.3 GPa, is observed just beneath the wheel. It is considered that this tensile stress causes the first crack initiation.

Figure 12 shows the FEA stress maps of σ_x in the *X-Z* plane during and after a static indentation of wheel. The maximum indentation load is 6.4 N. Although the three-dimentional FEA calculation was performed to determine the stress field, the two-dimensional (*X-Y* plane) stress maps at the center of the wheel are shown in Figure 12. In Figure 12, the blue and red regions represent compressive and tensile stresses, respectively. On loading (Figure 12A), the maximum tensile stress is 1.09 GPa. It is considered that FEA calculation can reproduce qualitatively the tensile stress which is also obtained from photoelastic image in Figure 11B. A considerable difference in the value of the maximum tensile stress between FEA and photoelasticity

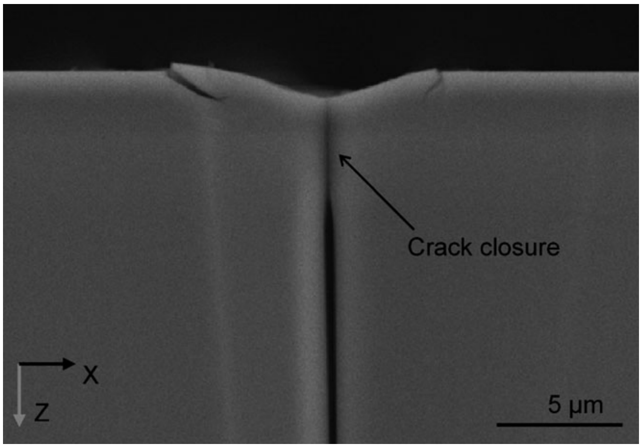

FIGURE 13 SEM image of the surface layer of glass after wheel scribing at 9.9 N

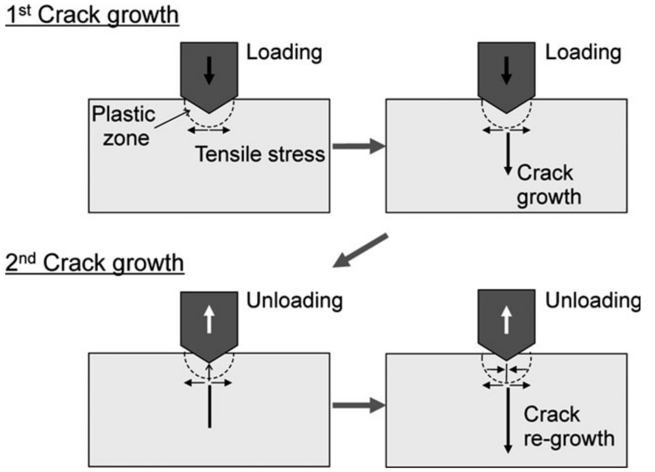

FIGURE 14 Schematic illustrations of the 1st and the 2nd cracks propagation during wheel scribing

probably may result from an assumption of two-dimensional stress field for photoelasticity and/or from the estimated values of parameters for plastic deformation of glass for FEA. After unloading (Figure 12B), the compressive stress still remains beneath the imprint of wheel, and the tensile stress also exists below this compressive region.

Figure 13 shows an SEM image of the cross-sectional plane perpendicular to the scribing groove. In Figure 13, there exists the region where the median crack is closed. Below the region of the crack closure, the crack-opening-distance becomes wider. It is considered that this crack closure results from the compressive stress which can be reproduced by FEA calculation as shown in Figure 12B. The compressive stress should exist in the plastic zone, because the compressive stress balances the tensile stress which can be estimated from the expanding cavity model as shown below.

Figure 14 shows schematic illustrations of cracking sequences during wheel scribing. Figures 14A and B represent the model of the first crack initiation during loading. Figures 14C and D show the model of the second crack propagation during unloading. During loading, the plastic zone is created beneath the wheel as shown in Figure 14A. The compressive stress in the plastic zone is balanced with the tensile stress outside the plastic zone (Figure 14A). The tensile stress causes the first crack to initiate (Figure 14B). During unloading process, on the other hand, a decrease in compressive stress beneath the wheel enables the crack to grow to the surface, or to the indenter (Figure 14C). Furthermore, because the tensile stress still remains at the bottom of plastic zone, the crack re-propagates as the second crack. The wider crack-opening-distance below the region of crack closure (Figure 13) also confirms an expansion of the plastic zone, which would be an origin of the tensile stress outside the zone and the balanced compressive stress inside the zone.

The stress fields estimated from FEA (Figure 12) and the model of the 1st and the second crack propagation (Figure 14) are supported by the CME model,[11] which explain that the tensile stress at the bottom of the plastic zone remains even after complete unload. However, the other authors have reported that the stress under the plastic zone changes from tensile on loading into compressive after unload.[4,10] Although the issue of the residual stress of glass after indentation or scribing is still controversial, further experimental and modeling works will be required in order to obtain more precise and quantitative stress field around the indentation or the scribing groove. It is expected that more information on glass plasticity could improve more efficient machining of a glass sheet using a scribing wheel.

5 | CONCLUSION

Through in-situ observation of cracking in glass during wheel scribing, it was clarified that the first crack initiates beneath the wheel and the second crack re-grows after passing through the wheel. In addition, the results of in-situ photoelastic measurement and FEA represented that the maximum tensile stress exists just beneath the wheel during loading. From an observation of the cross-section of a scribing groove, it was found that a part of the median crack was closed in the plastic zone. It is considered that the tensile stress at the bottom of the plastic zone causes the origin of the first crack initiation, and that the compressive stress in the plastic zone is the origin of the closure of the median crack.

REFERENCES

1. Ono T, Tanaka K. Theoretical and quantitative evaluation of the cuttability of AMLCD glass substrates using a four-point-bending test. *J Soc Inf Disp*. 1999;7:207-212.
2. Kondrashov VI, Shitova LA, Litvinov VA, Surkov VV. Characteristics of cutting parameters and their effect on the glass edge quality. *Glass Ceram*. 2001;58:303-305.
3. Hagan JT, Swain MV. The origin of median and lateral cracks around plastic indents in brittle materials. *J Phys D Appl Phys*. 1978;11:2091-2102.
4. Cook RF, Pharr GM. Direct observation and analysis of indentation cracking in glasses and ceramics. *J Am Ceram Soc*. 1990;73:787-817.
5. Lawn BR, Swain MV. Microfracture beneath point indentations in brittle solids. *J Mater Sci*. 1975;10:113-122.
6. Sglavo VM, Green DJ. Subcritical growth of indentation median cracks in soda-lime-silica glass. *J Am Ceram Soc*. 1995;78:650-656.
7. Kopchekchi LG, Shitova LA. Initiation and propagation of cracks in glass beneath a disc cutter. *Glass Ceram*. 1996;53:107-109.
8. Lawn BR, Evans AG. A model for crack initiation in elastic/plastic indentation fields. *J Mater Sci*. 1977;12:2195-2199.

9. Tanaka K. Elastic/plastic indentation hardness and indentation fracture toughness: the inclusion core model. *J Mater Sci*. 1987;22:1501-1508.
10. Yoffe EH. Elastic stress fields caused by indenting brittle materials. *Philos Mag A*. 1982;46:617-628.
11. Chiang SS, Marshall DB, Evans AG. The response of solids to elastic/plastic indentation. I Stress and residual stresses. *J Appl Phys*. 1982;53:298-311.
12. Hagan JT. Shear deformation under pyramidal indentations in soda-lime glass. *J Mater Sci*. 1980;15:1417-1424.
13. Swain MV. The deformation associated with the scoring of soda-lime float glass with a disc cutter. *Glass Technol*. 1980;21:290-296.
14. Swain MV. Median crack initiation and propagation beneath a disc glass cutter. *Glass Technol*. 1981;22:222-230.
15. Ono T, Tanaka K. Effective of scribing wheel dimensions on the cutting of AMLCD glass substrates. *J Soc Inf Disp*. 2001;9:87-94.
16. Swain MV, Metras JC, Guillemet CG. A deformation and fracture mechanics approach to the scoring and breaking of glass. *J Non-Cryst Solids*. 1980;38&39:445-450.
17. Smirnov MI, Spiridonov YA, Karapetyan AR. Modern sheet-glass cutting technologies. *Glass Ceram*. 2011;68:6-7.
18. Litvinov VA, Maistrenko IA, Tarasov EA, Grinberg FB. Cutting glass with a hard- alloy roller. *Steklo Keram*. 1972;12:793-795 (Translated into English).
19. Cook RF. Deformation and fracture by sharp rolling contacts. *J Am Ceram Soc*. 1994;77:1263-1273.
20. Koike A, Akiba S, Sakagami T, Hayashi K, Ito S. Difference of cracking behavior due to Vickers indentation between physically and chemically tempered glasses. *J Non-Cryst Solids*. 2012;358:3438-3444.
21. Yoshida S, Iwata S, Sugawara T, et al. Elastic and residual stresses around ball indentations on glasses using a micro-photoelastic technique. *J Non-Cryst Solids*. 2012;358:3465-3472.
22. Matsusaka S, Mizubuchi G, Hidai H, Chiba A, Morita N, Onuma T. Observation of crack propagation behavior and visualization of internal stress field during wheel scribing of glass sheet. *J Jpn Soc Precis Eng*. 2015;81:270-275. (in Japanese).
23. Giannakopoulos AE, Suresh S. Determination of elastoplastic properties by instrumented sharp indentation. *Scr Mater*. 1999;40:1191-1198.
24. Lemaitre J, Chaboche JL. *Mechanics of Solid Materials*. UK: Cambridge University Press; 1990, 198-205.
25. Aben H, Guillemet C. *Photoelasticity of Glass*. Berlin, Germany: Springer; 1993, 51-78.

How to cite this article: Tomei N, Murakami K, Fukunishi T, Yoshida S, Matsuoka J. Direct observation of crack propagation in a liquid crystal display glass substrate during wheel scribing. *Int J Appl Glass Sci*. 2017;00:1-9. https://doi.org/10.1111/ijag.12272